Assessment of the mesoscale structures observed by gliders during the CINEL project

by

L.E. Sitz[1], E. Mauri[1], R. Gerin[1], P-M. Poulain[1], D. Hayes[2]

[1]OGS, Trieste, Italy

[2]UCY, Nicosia, Cyprus

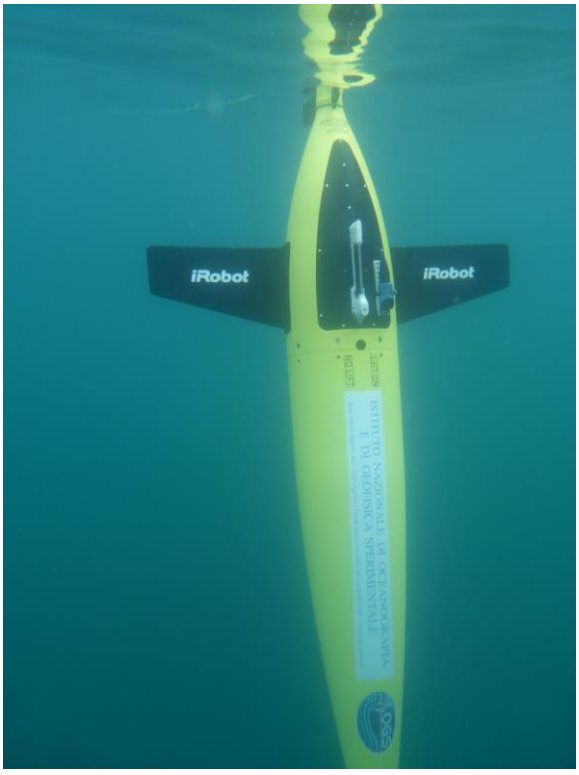

Approved for release by:.. .....

Dr. Paola Del Negro

Director, Oceanography Section

Table of Contents

1. Introduction

The Levantine Sea is the easternmost part of the Mediterranean Sea and it is the largest semi-enclosed water body on Earth, located at mid latitude. The region under analysis in this report is the eastern Levantine sub-basin (LSB) located between 32°E and 36°E, and 35°N and 32°N. The circulation in this area is dominated by an along-slope anticyclonic current named the Libyo-Egyptian Current (Millot and Taupier-Letage, 2005; Gerin et al., 2009; Millot and Gerin, 2010) extending as a northward current along the Middle-East coast, a central eastward cross-basin meandering current named Mid-Mediterranean Jet (MMJ) flowing from ~24°E to southeast of Cyprus (Pinardi et al., 2006; Zodiatis et al., 2010; and Pinardi et al., 2011), and a series of mesoscale features, including two recurrent eddies: the Cyprus Eddy (CE) and the Shikmona Eddy (ShE) (Menna et al, 2012). The CE is an anticyclonic eddy with a recurrent dynamic feature characterized by seasonal variability in shape, dimension and position (Zodiatis et al., 2005, Menna et al., 2012). The ShE represents a complex system, composed of several cyclonic and anticyclonic eddies, in which the positions, sizes and intensities vary markedly (Ayoub et al.,1998; Zodiatis et al.,1998; Gertman et al., 2007; Menna et al. 2012).

The thermohaline structure of this sub-basin is characterized by a well-developed (in the warm season) Levantine Surface Water (LSW), with temperature values between 22 and 28 °C and salinity of 39 to 39.6 PSU; advected Atlantic Water (AW) with temperature values of 18 to 22 °C and salinity between 38.6 and 39.2 PSU, and Levantine Intermediate Water (LIW) formed when LSW cools down and sinks along isopycnals to intermediate depth (ca. 130 m < z < 350 m), with typical values of 15 to 17.5 °C and 38.95 to 39.3 PSU (Ozer et al., 2016).

This report focuses on the analysis and examination of the mean features governing the dynamics of the LSB, using glider data. The observations correspond to the missions conducted in the frame of the CINEL project, from September 2016 to September 2017. In particular, we examine the physical properties of the cyclonic and anticyclonic structures developed in the region of the CE and ShE formation, sampled by the gliders.

The goal of the CINEL project was to measure the currents and water mass properties in the north-eastern areas of the Levantine Basin in order to study the complex circulation features

governing the dynamics in the area. The measurement program in the north-eastern Levantine, with focus on the area south of Cyprus and off the Israeli coast included in-situ observations from gliders, floats, and drifters, and it was separated into fall and winter phases in order to investigate seasonal variability. To identify the various missions in this report we have sorted the campaigns chronologically and named them from C1 to C5 (Table 1).

2. Data and methods

Three Seagliders were operated by UCY and OGS during CINEL: SG149, SG150 and SG554. The Seaglider is an autonomous instrument designed to measure water properties in the top 1000 m of the water column and equipped with CTD (pumped in the case of SG554), oxygen, chlorophyll florescence and turbidity sensors. In this project, temperature and salinity were collected in the top 950 m of the water column in all five campaigns. Oxygen, chlorophyll and turbidity measurement stopped respectively at 600 m depth and for the last two at 300 m (for further details, see Appendix). The gliders were deployed in two different seasons: the first in fall 2016 and the other in winter 2017 (Table 1). During the first period, three glider campaigns were organized.

Glider ID	**Phase**	**Deploy time**	**Lat N**	**Lon E**	**Recovery time**	**Lat N**	**Lon E**
C1:SG150	I (fall)	31/08/16 06:48	34.965	33.999	17/10/16 23:44	34.555	33.762
C2:SG554	II (fall)	19/10/16 07:16	34.914	34.001	07/12/16 08:56	34.927	34.034
C3:SG149	II (fall)	04/11/16 08:57	34.930	34.012	06/12/16 12:35	34.907	33.998
C4:SG149	III (winter)	10/02/17 09:38	34.902	34.005	13/03/17 22:44	33.628	33.525
C5:SG554	III (winter)	10/02/17 10:45	34.897	34.014	16/03/17 08:33	34.929	34.007

Table 1: Information about the gliders deployed during CINEL.

The first mission (C1) began on 31 August with the deployment of SG150. On 17 October 2016, SG150 was recovered and SG554 glider was deployed (C2). The SG149 glider (C3) was launched on 4 November 2016. C2 mission ended on 7 December 2016 while C3 ended on 6 December 2016. Fig. 1 (a) shows the trajectories of all CINEL gliders. Figures 1 (b) to (f) show the evolution in time of every trajectory (ordered chronologically), with blue colors indicating the initial measurements and red colors showing the final observations. C2 and C3 trajectories

had a proximity point on 3 December (C2: 33.911E°/34.572°N vs C3: 33.924°E/34.576°N) with only 1 hour of delay between passages.

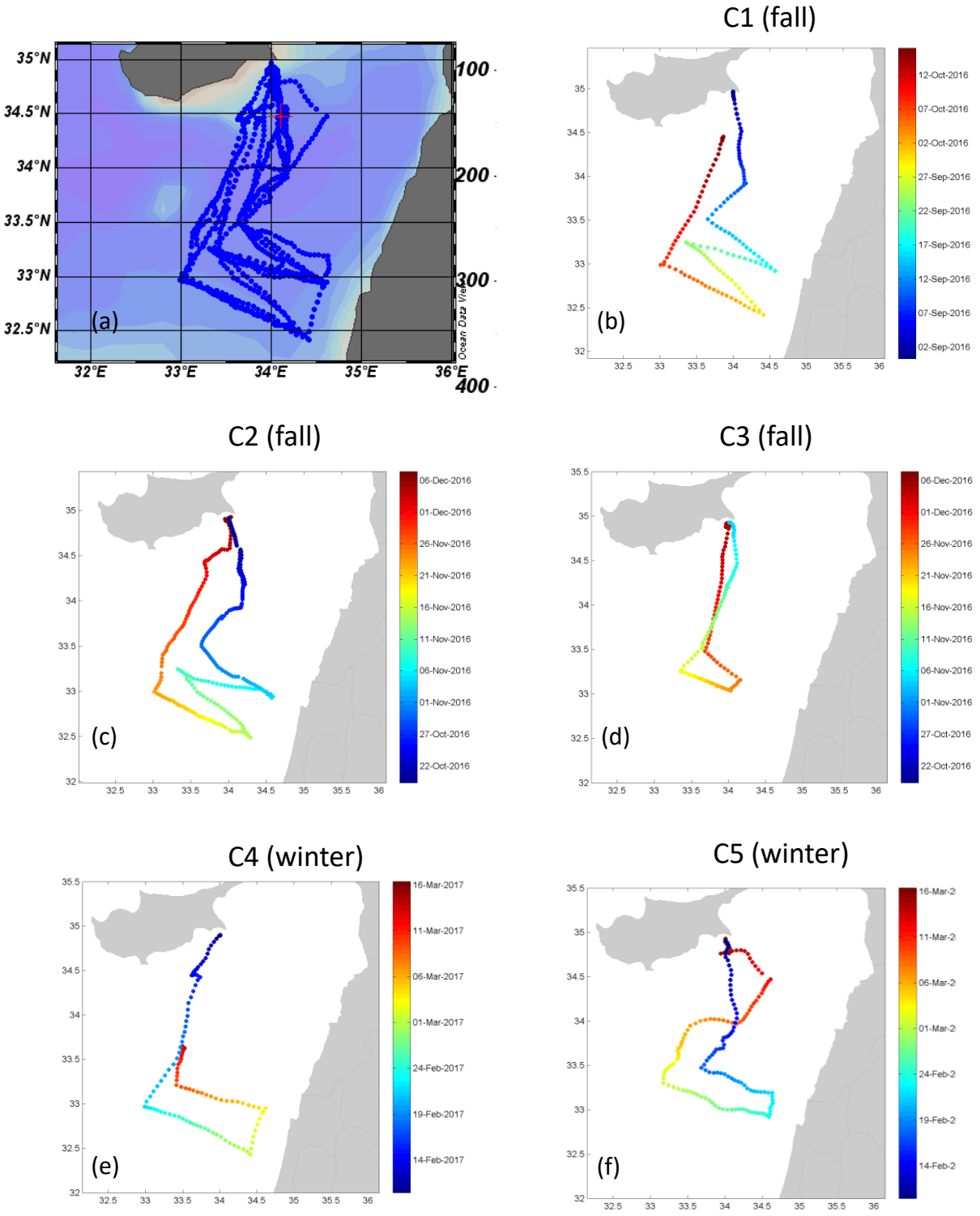

Figure 1: (a) Glider tracks during the CINEL missions: (b) **C1**:SG150 (fall); (c) **C2**:SG554 (fall), (d) **C3**:SG149 (fall); (e) **C4**:SG149 (winter); (f) **C5**:SG554 (winter). Colors represent the evolution in time of each trajectory, with blue colors indicating the initial measurements and red colors showing the final observations.

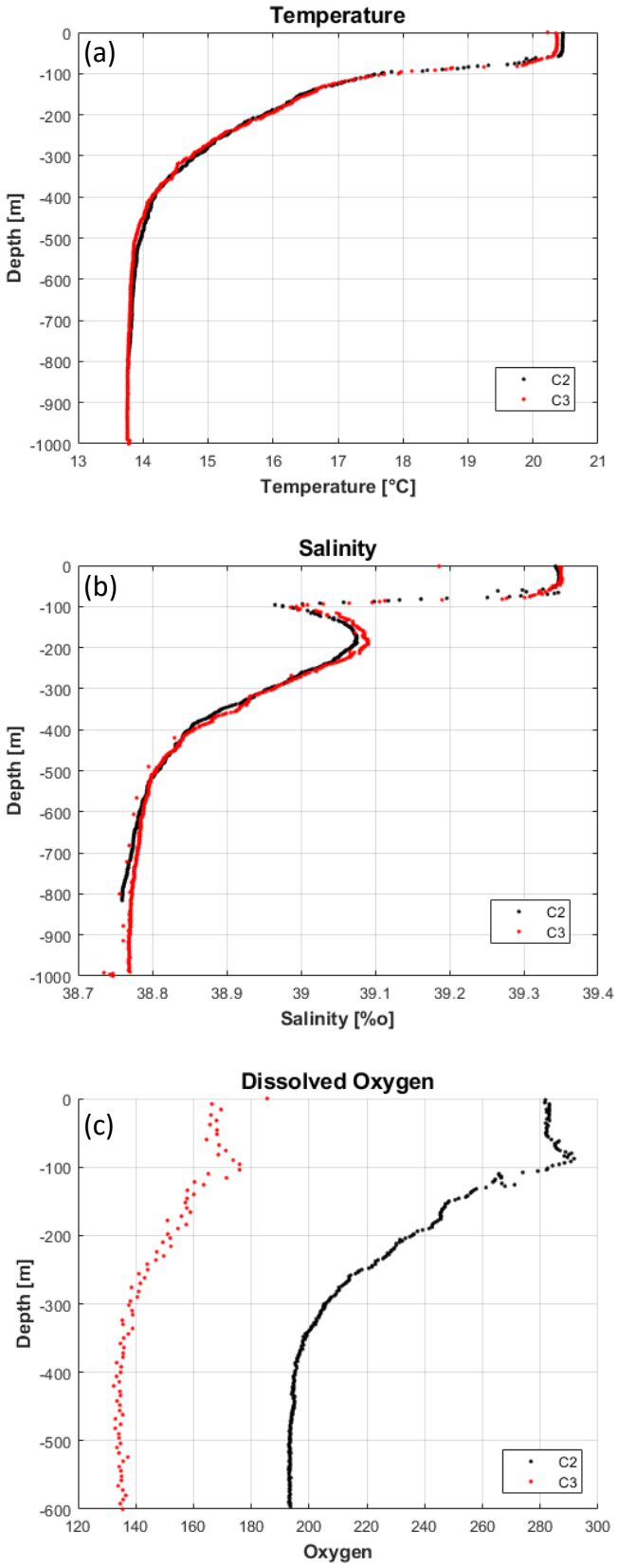

Figure 2: Comparison of the (a) temperature, (b) salinity and (c) dissolved oxygen profiles, for the C2 (black dots) and C3 (red dots) missions on December, 3. During this day, glider trajectories passed through the same region with only 1 hour of difference.

Fig. 2 (a) and (b) shows the temperature and salinity profiles in the respective positions (C2 black dots and C3 red dots), showing a coincidence in the calibration of CTD sensors. On the other hand, Fig. 2 (c) is the comparison of the oxygen profile in the same position, showing that for this variable further processing is needed in order to compare the results of the different missions. In winter, SG149 (C4) and SG554 (C5) were launched on 10 February 2017. SG554 was recovered on 16 March 2017, in the vicinity of the coastal deployment point, while SG149 was recovered on 13 March 2017 after a premature battery failure. The observations of SG149 and SG150 were processed by UCY. The observations obtained from SG554, after the first quality control, were processed eliminating values out of range and spikes, and binned vertically (using the average value) to distribute them to uniform non-overlapping levels of 2 m depth. For all the glider campaigns, in this report, we analyze only the observations obtained from the upcast. This decision was made, taking into account the fact, that the profiles, due to the glider sampling design, miss the top 20 to 30 m (see Appendix).

3. Main results

a. The Cyprus Eddy (CE)

To assess the anticyclonic structures developed in the region of CE formation (Menna et al. 2012), a series of vertical transects of temperature and salinity fields were analyzed.

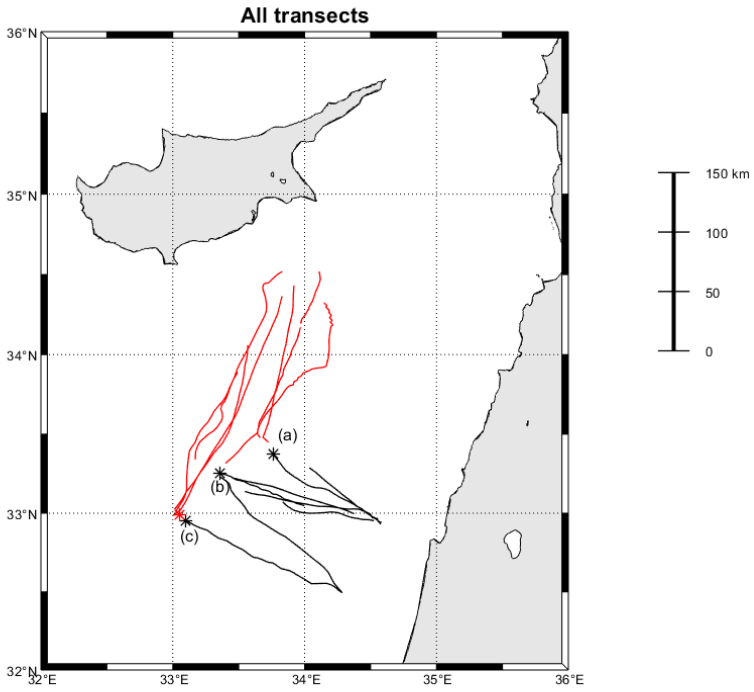

Figure 3: Selected transects from all the glider campaigns. In red the coincident ones with the region of CE, in black those corresponding to the region of ShE.

The used data were selected using the following criteria: inspecting the satellite Absolute Dynamic Topography (ADT) fields and their corresponding geostrophic currents, dates in which the glider crossed through an anticyclonic structure in the region of interest were identified. The red lines in Fig. 3 show the transects corresponding to the data of the selected stations. The red asterisk is the starting point of the southernmost trajectory crossing the anticyclonic eddy. All the transects in the CE region have been plotted in function of the distance, using this point as absolute reference. In order to identify the different structures, we have numbered the transects chronologically (Fig. 4).

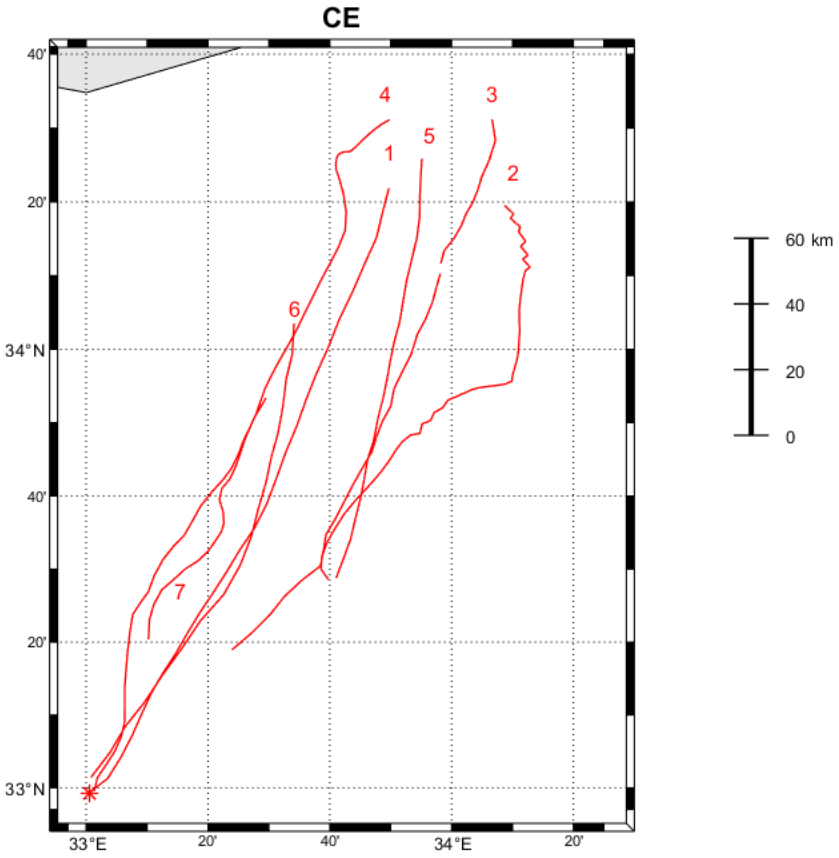

Figure 4: Transects corresponding to anticyclonic structures, present in the CE region, numbered chronologically.

Figures 5 to 7 show the temperature (left) and salinity (right) fields of each transect, chronologically sorted. Notice that even when some of the transects have been sampled from south to north and the others in the opposite direction, all the transects are oriented so that the southernmost point of the transect is always on the left in the plot.

The gliders crossed through anticyclonic structures five times in autumn (Fig. 5 a-f and Fig. 6 a-d) and twice in winter (Fig. 7 a-d).

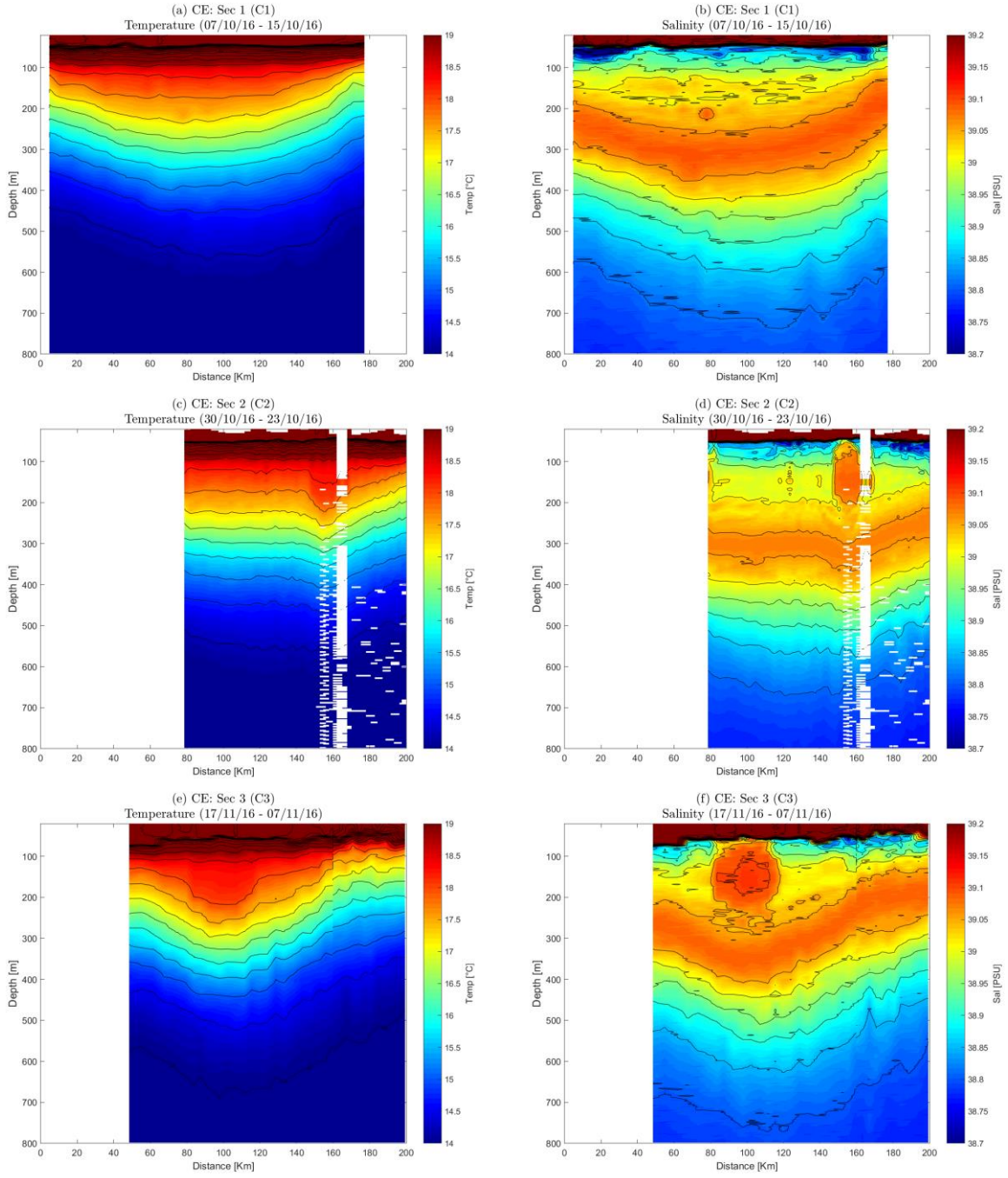

Figure 5: Temperature (left) and salinity (right) transects in the region of CE (transects 1 to 3).

Transect 2 (Fig. 5 c and d) covers a region of an anticyclonic gyre located further east (probably the North Shikmona Eddy, Fig. 8 a), but as days pass by it merges with another anticyclone developed in the location of CE, forming a bigger and stronger anticyclonic structure (see ADT map, Fig. 8 b). This strong structure is observed in transect 3 (Fig. 5 e and f). It is worth

mentioning that transects 4 and 5 have a period of temporal coincidence and they show different regions of the same anticyclone (Fig 6 a-d).

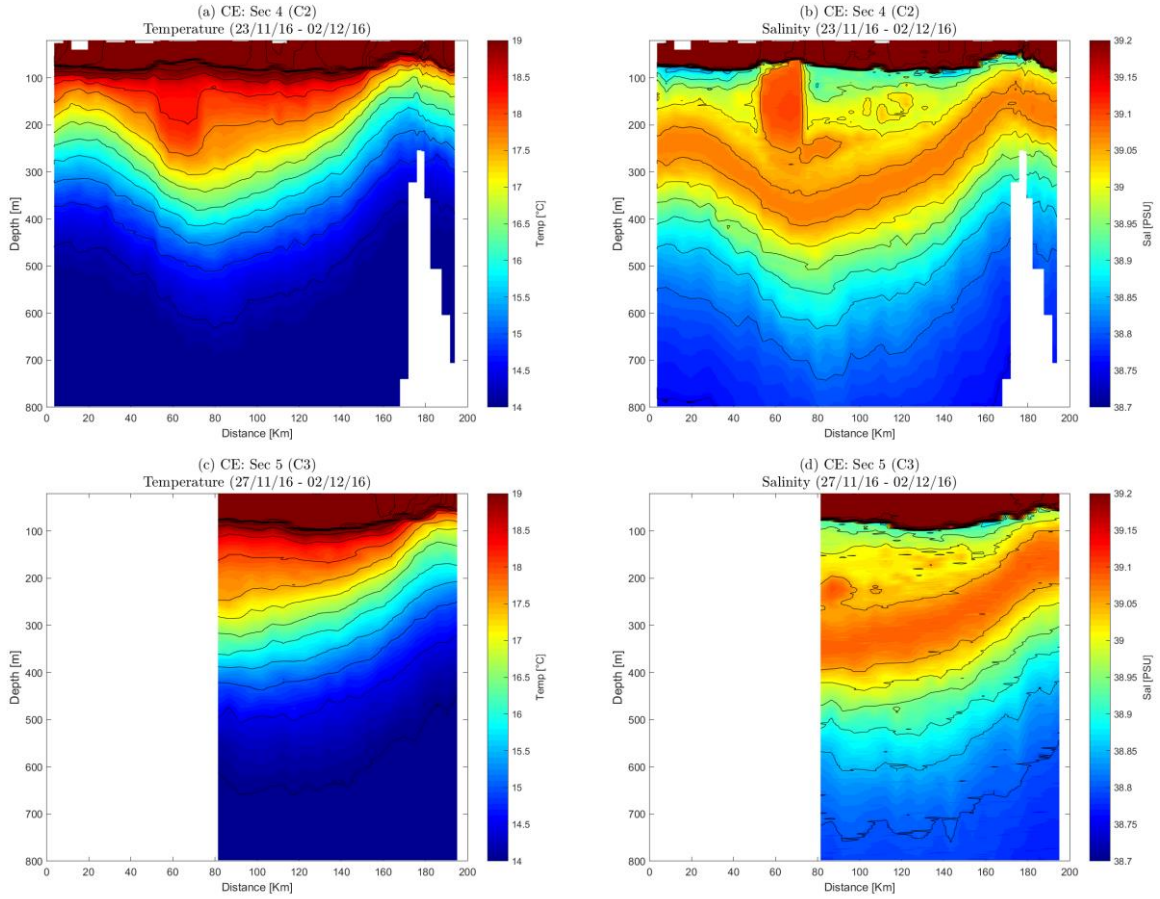

Figure 6: Temperature (left) and salinity (right) transects in the region of CE (transects 4 and 5).

The ADT field evidences a positive anomaly in the center of all the structures, in correspondence with the anticyclonic circulation (e.g. Fig. 8). On the other hand, the SST field shows a maximum of temperature over the anticyclonic formation only during winter, when the thermocline is not present (not shown). The vertical fields of temperature and salinity (Figs. 5, 6 and 7) show a clear doming in the central part of the structure, reaching a maximum depth of 700 m both in autumn and winter. In these observations, the horizontal extension is higher in autumn with a maximum diameter of ~180 km, while the diameter of the winter structures is less than 140 km.

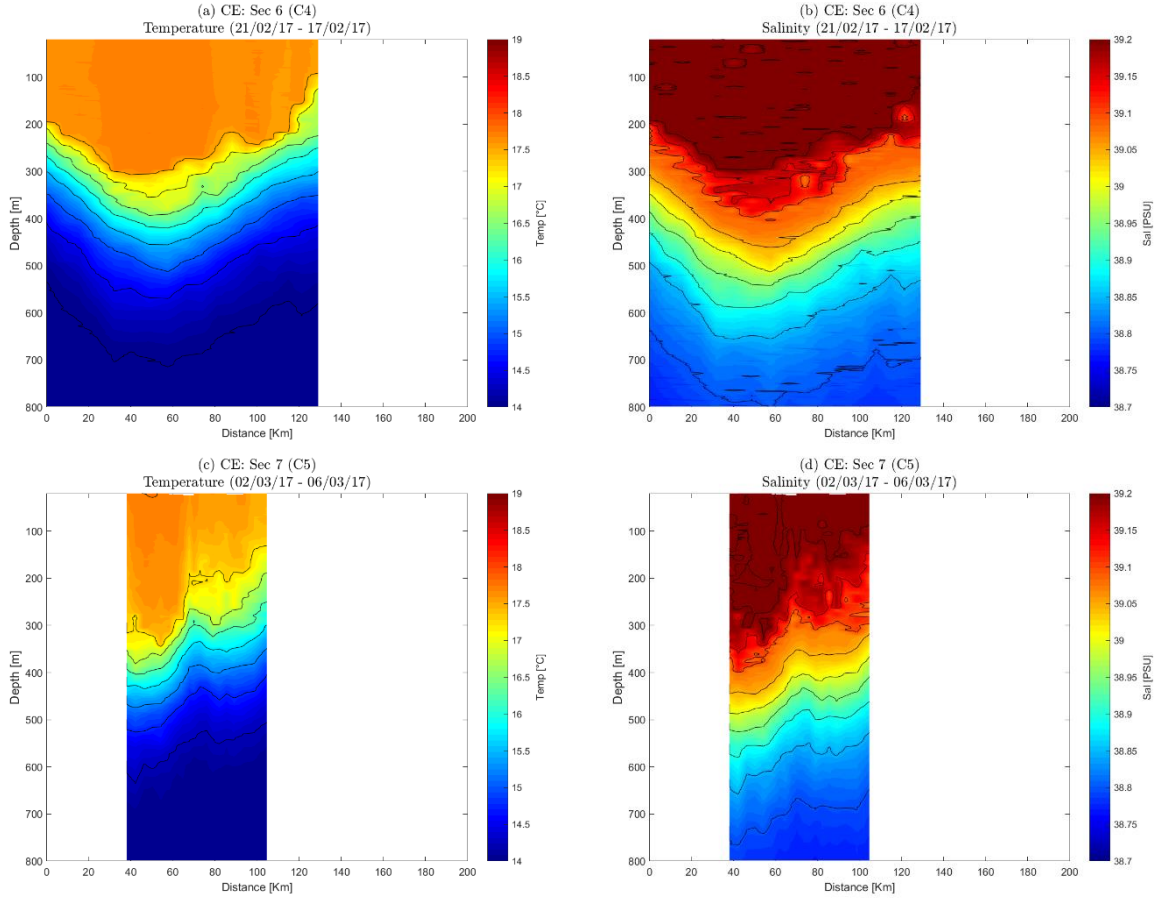

Figure 7: Temperature (left) and salinity (right) transects in the region of CE (transects 6 and 7).

Fig. 9 shows the TS diagram corresponding to the transects in Figs. 5, 6 and 7. During autumn, the presence of LSW near the surface and AW underneath the LSW is observed. The presence of AW is also evident in the vertical transects of salinity during the fall missions (Fig. 5 b, d, f and Fig. 6 b, d), where there is a minimum of salinity right under the thermocline (between 50 and 100 m depth) that weakens as winter comes. Furthermore, during autumn a maximum of salinity between 200 and 300 m corresponding to the LIW is observed. This maximum does not appear in winter, because in this period the vertical mixing reaches 300 m depth. However, the TS diagram (Fig. 9) shows that all the campaigns captured water masses with features similar to the LIW (Ozer et al, 2017).

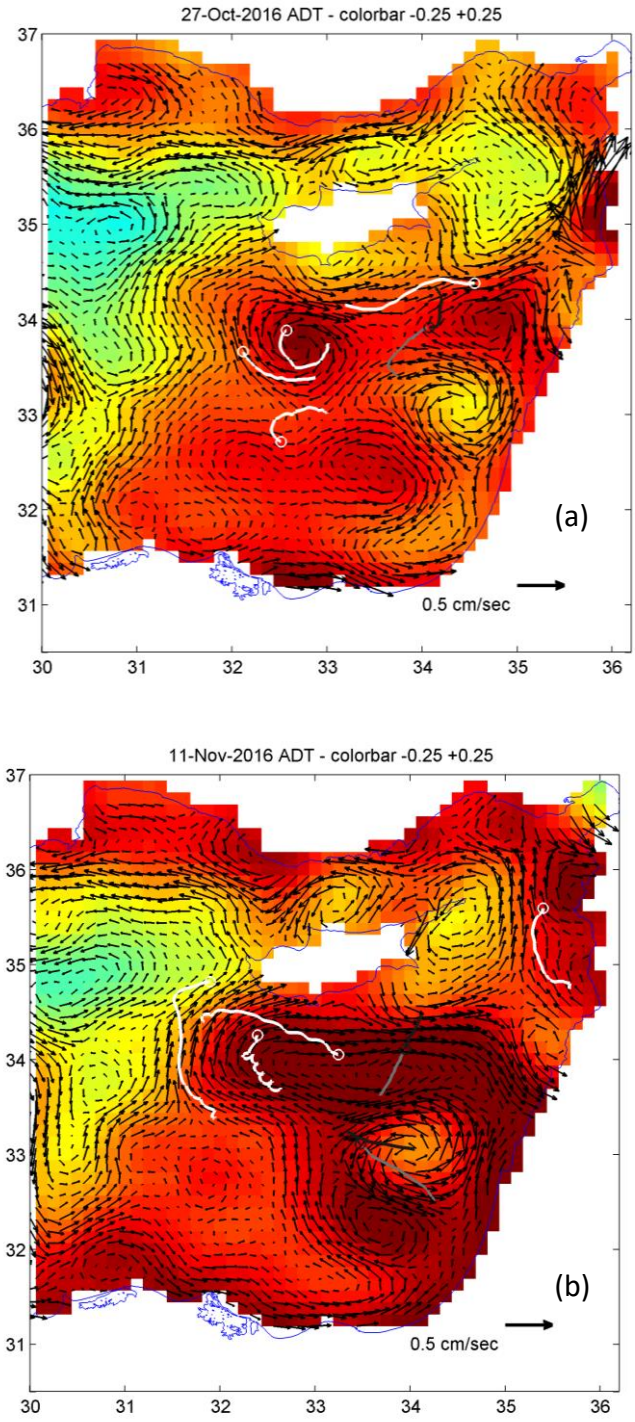

Figure 8: ADT field and geostrophic currents for (a) 27/11/2016 and (b) 11/11/2016. White lines correspond to drifter tracks launched during this period while black lines are glider tracks.

It is interesting to note the presence of a high salinity subsurface core in Fig. 5 d, f and Fig. 6 b, located in the central zone of the anticyclonic gyre. The location of the core is coincident with the location of a region of lower oxygen (not shown), and its values are similar to the LIW

salinity. The existence of this high salinity core has been reported previously in Hayes et al. (2016) from observations obtained in a glider mission which took place from 16/12/2011 to 01/06/2012. However, during this period, the core was located between 200 and 400 m depth.

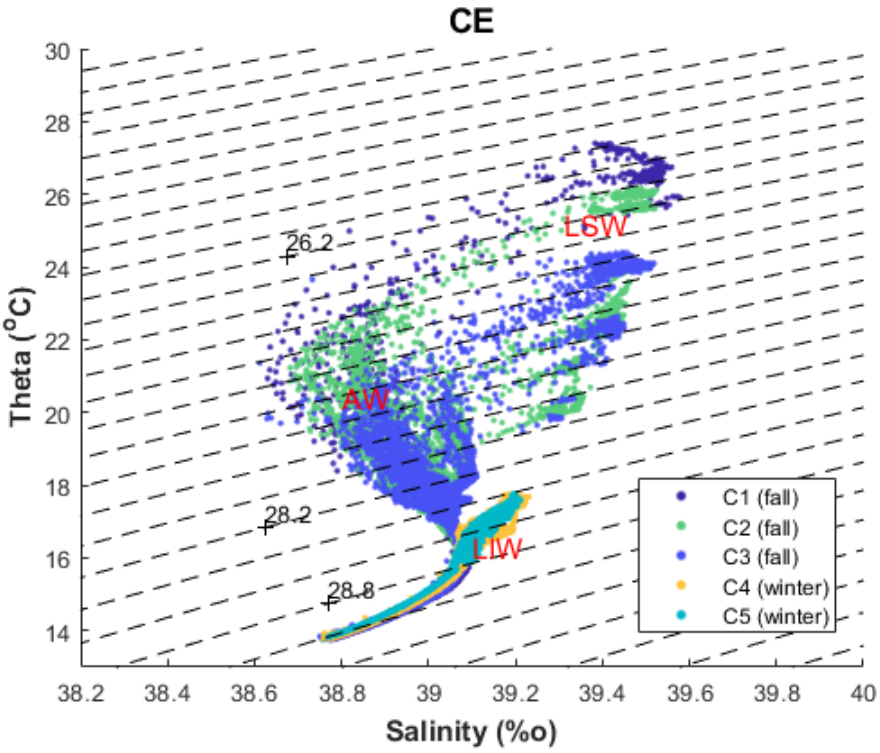

Fig. 9: TS diagram for the stations corresponding to the transects shown in Figs. 5 to 7.

b. The Shikmona Eddy (ShE)

The transects used to study the cyclonic structure corresponding to the region of ShE have been derived using the same criteria described before for the CE. Fig. 3 shows all the selected transects in the ShE region (black lines). As for the CE region, we have numbered the transect chronologically to identify the location of the different structures (Fig. 10). In this case we have selected three reference points in order to compare better the structure dimension and relative position. These reference points are identified in Fig. 3 by a letter and a black asterisk, and were used as follows: (a) reference point of transects 1 and 3; (b) reference point of transects 2, 4, 5, 7 and 8; (c) reference point of transect 6.

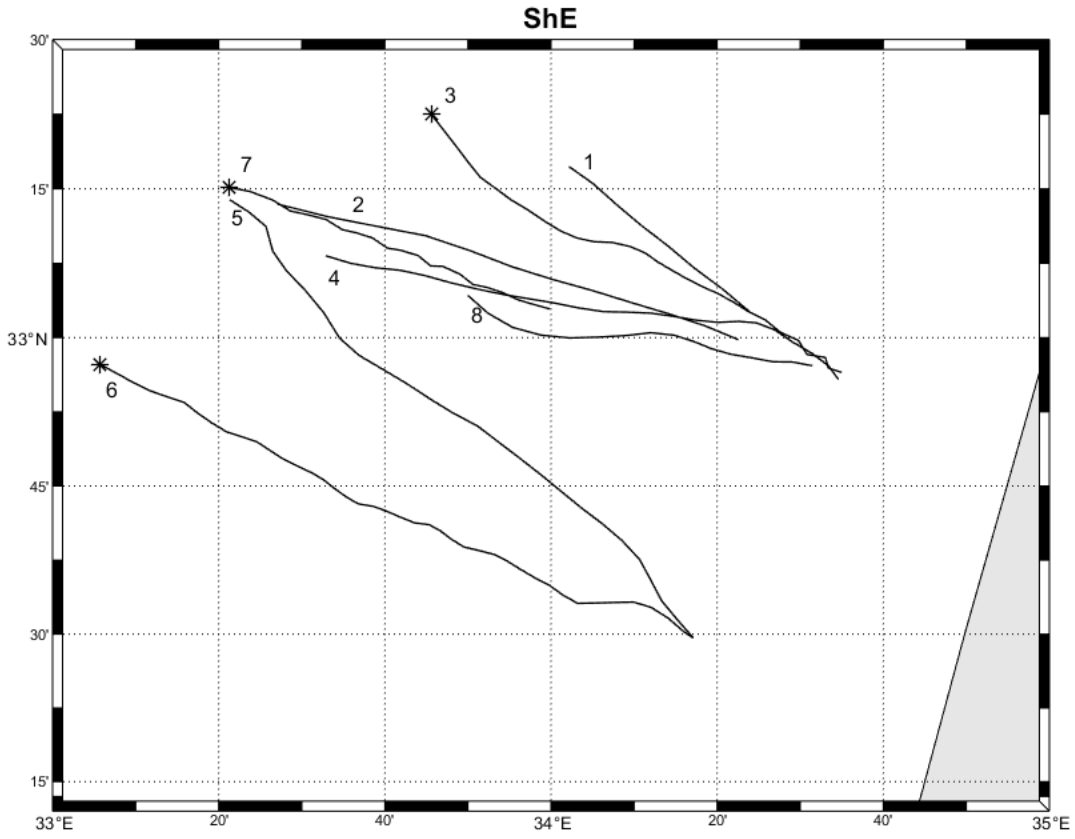

Fig 10: Transects corresponding to cyclonic structures, present in the ShE region, numbered chronologically.

The transects in Figs. 11 to 13 are oriented so that the westernmost point of the transect is on left in the plot. Transect 1 and 2 (Fig 11 a-d) correspond to the same small cyclonic structure, with a weak geostrophic current related to it (not shown). In this case, the doming corresponding to the center of the cyclone seems to be shifted towards west with respect to that observed in the ADT field (not shown). For this structure a maximum of salinity corresponding to the LIW between 200 and 300 m depth can be observed.

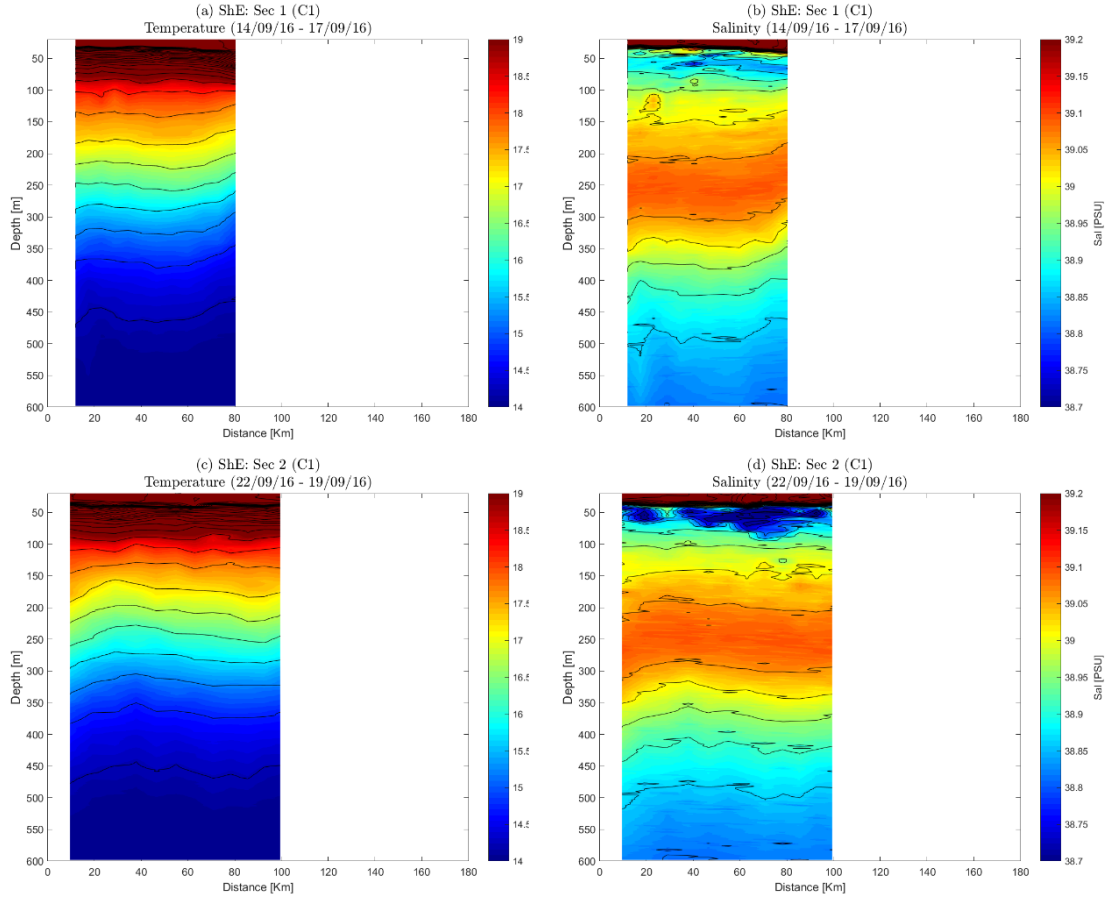

Figure 11: Temperature (left) and salinity (right) transects in the region of ShE (transects 1 and 2).

Transects 3 to 7 (Fig. 11 and Fig. 12 a-b) correspond to a single cyclonic formation (crossed through by the gliders during the C2 and C3 missions), with a strong geostrophic current and a pronounced central valley (Fig. 14). In this case, the doming on the central part of the structure - and below the thermocline - is quite evident. The diameter of this anticyclone is ~100 km, while the maximum of salinity corresponding to the LIW is between 150 and 250 m depth.

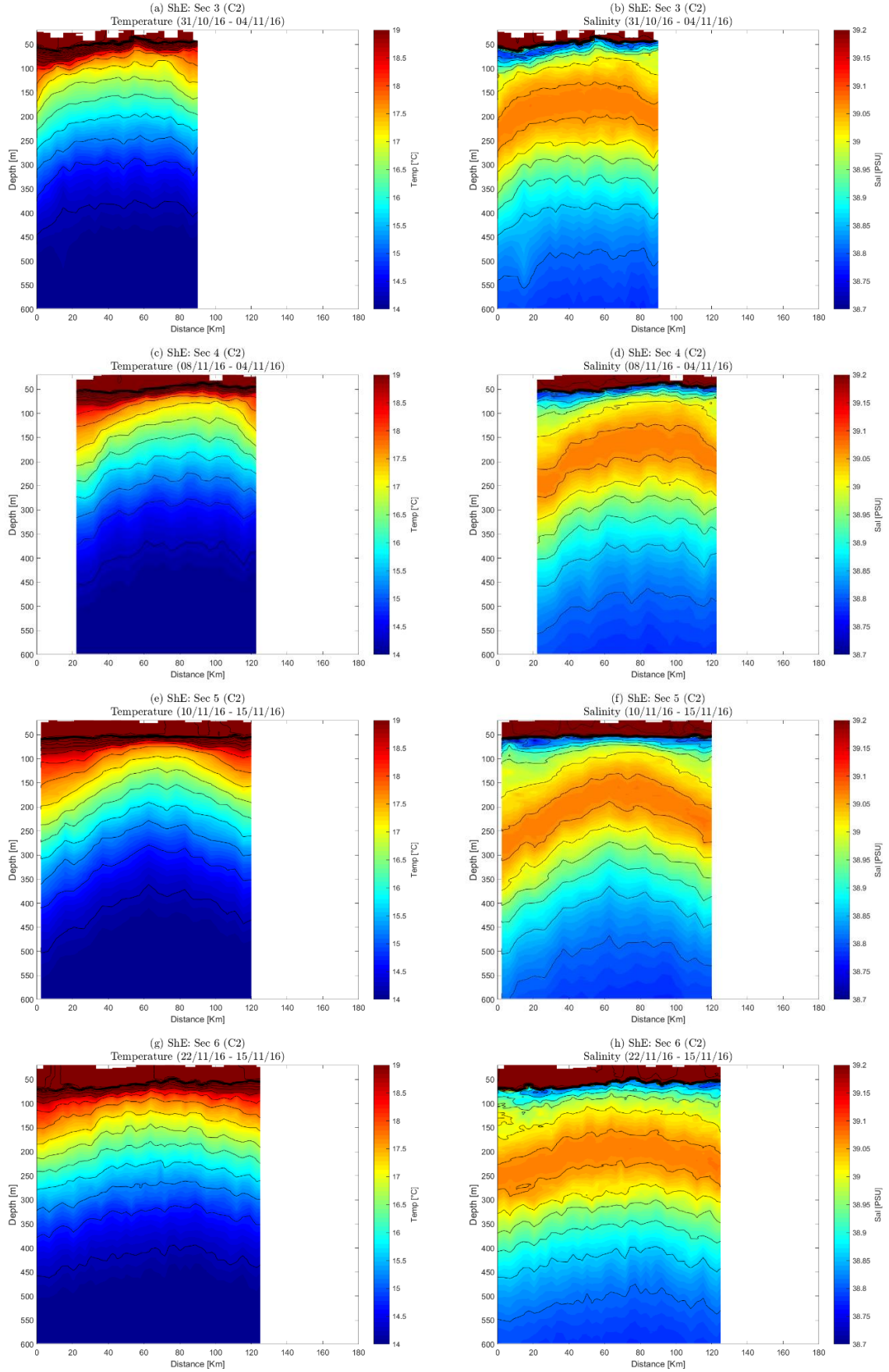

Figure 12: Temperature (left) and salinity (right) transects in the region of ShE (transects 3 to 6).

Finally, the only cyclonic structure captured during the winter (Fig. 13 c-d) is rather small, with a diameter less than 70 km, and shows a weak geostrophic current. The central doming is very pronounced, probably intensified by the vertical mixing, and a maximum of salinity related to the LIW cannot be observed.

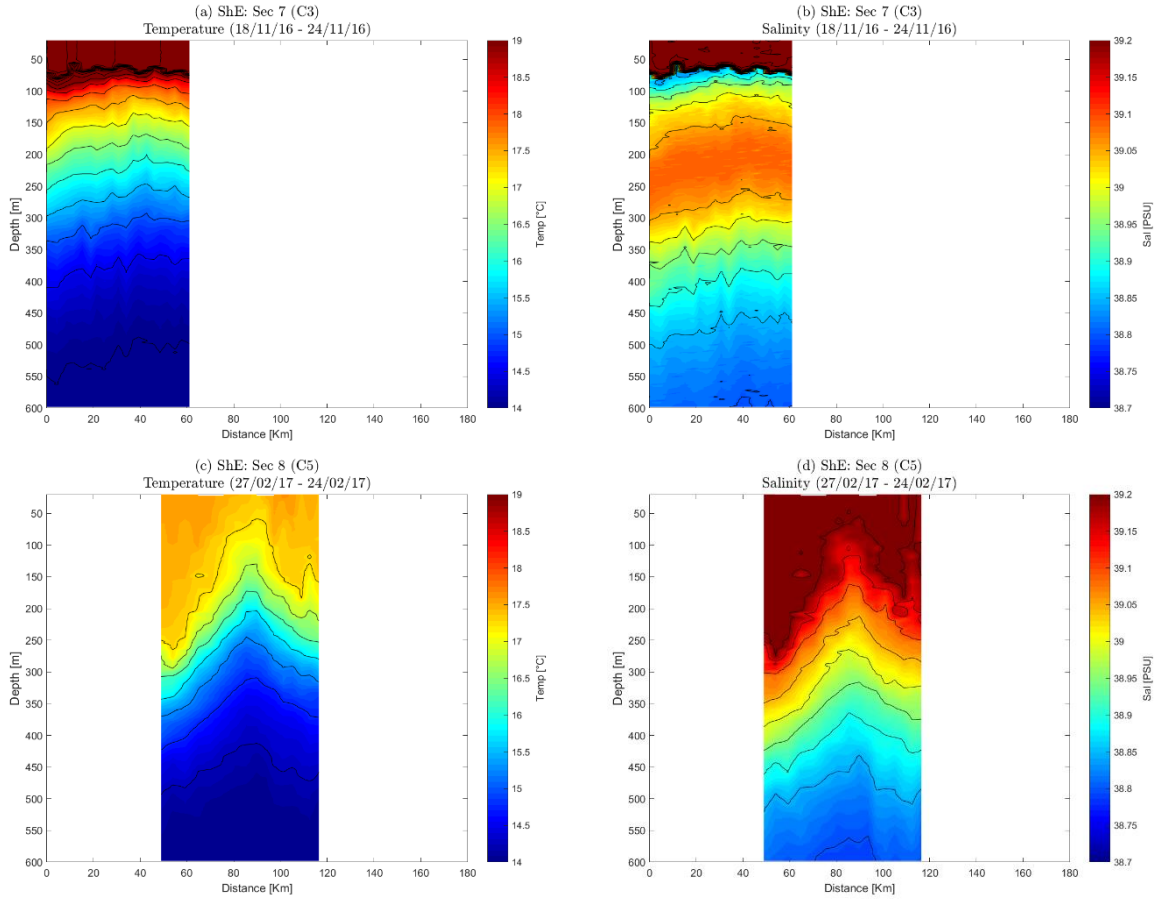

Figure 13: Temperature (left) and salinity (right) transects in the region of ShE (transects 7 and 8).

The TS diagram corresponding to the region of ShE formation (Fig. 15) shows less dispersion in the superficial and sub-superficial waters for all three fall missions, in comparison to the CE region (Fig. 9). Furthermore, during the C1 mission the near surface waters captured were warmer than the observed in the C2 and C3 campaigns, while its salinity is similar in all the three cases. On the other hand, the highest temperatures reached in surface during winter over this area, are lower than those observed in the CE region for each respective mission.

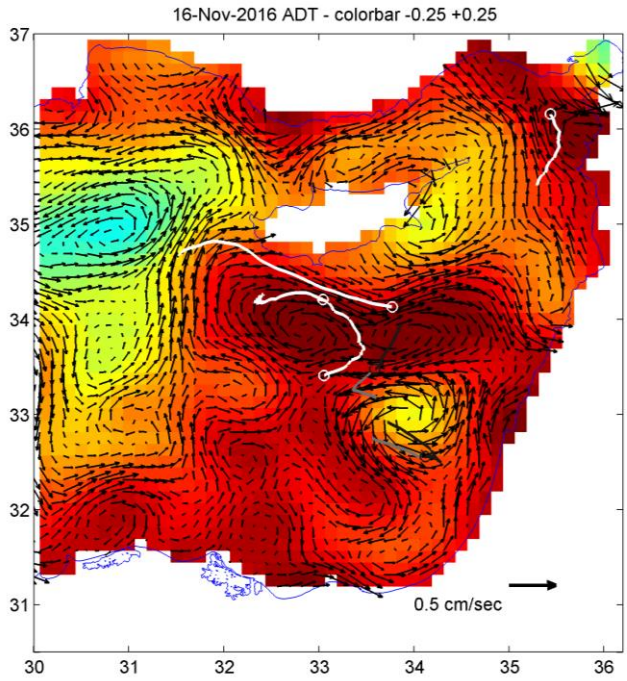

Figure 14: ADT field and geostrophic currents in 16/11/2016. White lines correspond to drifter tracks launched during this period while black lines are gliders tracks. A strong geostrophic current and a pronounced central valley is evidenced in the cyclonic structure observed in different transects (numbers 3 to 7) over the region of ShE formation.

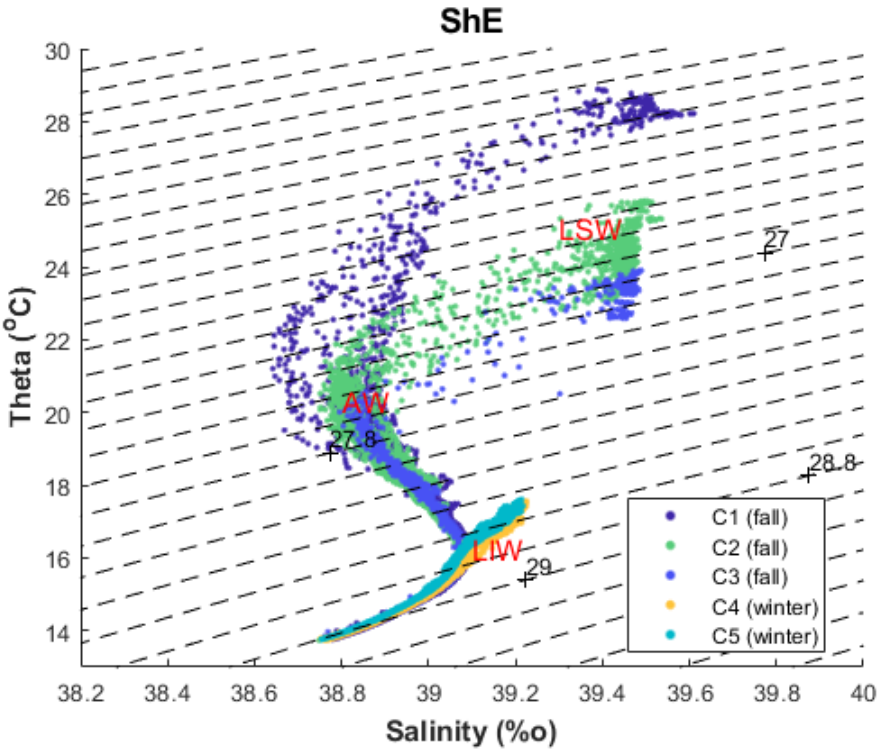

Figure 15: TS diagram in the region of ShE formation for all the five missions.

The thermohaline structure in deeper levels is similar to all the campaigns and also similar to the one observed in the CE area.

4. Conclusions

We have examined the temperature and salinity fields of the cyclonic and anticyclonic structures developed in the region of the CE and ShE formation, measured by the gliders deployed during the CINEL project.

- During the five missions, 6 anticyclonic structures in the CE area and 4 cyclonic gyres in the region of ShE were captured (in the case of CE one single structure was captured twice, while in the ShE region one single structure was captured five times).
- The ADT field evidences a positive anomaly in the center of all the anticyclonic structures, and a negative anomaly for most of the cyclonic formations. In this latter case however, the doming corresponding to the center of the cyclone in the first two transects, seems to be shifted towards the west with respect to that observed in the ADT field.
- The vertical fields of temperature and salinity corresponding to the CE region show a clear doming in the central part of the structure, reaching a maximum depth of 700 m both in autumn and winter.
- In the anticyclonic structures captured between 23 October and 2 December, a subsurface high salinity core located in the central zone of the anticyclonic gyre was identified, with values similar to the LIW salinity. This core has been reported in previous observations (Hayes et al., 2016).

Warm and salty LSW is found in both CE and ShE regions, which gradually cools and freshens throughout the missions. During autumn AW is found at depths just below LSW, revealed as a local minimum in salinity, which is slowly destroyed as the summer season comes to an end in December. LIW is found at depths from below the AW down to approximately 200 to 300 m and it is indicated by a relative maximum in salinity.

During the winter missions, warm and salty LSW is cooled to less than 18 °C and it is deeper than 200 m. AW is no longer visible as a local minimum in salinity, having been mixed with the layers below and above during the winter in the weeks prior and during the mission (January-

March). Neither is LIW any longer identifiable as a relative maximum in salinity, but it has mixed with the LSW and AW to form a deep mixed layer of about 200 m which could be thought of as new LSW.

5. References

Ayoub, N., Le Traon, P.Y., De Mey, P., 1998. A description of Mediterranean surface variable circulation from combined ERS-1 and TOPEX/POSEIDON altimetric data. J. Mar. Syst. 18, 3–40.

Gerin, R., Poulain, P.-M., Taupier-Letage, I., Millot, C., Ben Ismail, S., Sammari, C., 2009. Surface circulation in the Eastern Mediterranean using Lagrangian drifters (2005–2007). Ocean Sci. 5, 559–574.

Gertman, I., Zodiatis, G., Murashkovsky, A., Hayes, D., Brenner, S., 2007. Determi- nation of the locations of southeastern Levantine anticyclonic eddies from CTD data. Rapp. Commun. Int. Mer. Mediterr. 38, 151.

Hayes, D.R., Dobricic, S., Gildor, H., 2016. Operational Assimilation of glider temperature and salinity in a mesoscale flow field: Eastern Mediterranean test case, Ocean Science Discussions 2016:1-27. DOI: 10.5194/os-2016-43.

Menna, M., Poulain, P-M., Zodiatis, G., Gertman, I., 2012. On the surface circulation of the Levantine sub-basin derived from Lagrangian drifters and satellite altimetry data. Deep- Sea Research I. 65 (2012) 46–58.

Millot, C., Gerin, R., 2010. The Mid-Mediterranean Jet Artefact. Geophys. Res. Lett. 37, L12602.

Millot, C., Taupier-Letage, I., 2005. Circulation in the Mediterranean Sea. Handb. Environ. Chem. 5 (K), 29–66.

Ozer, T., Gertman, I., Kress, N., Silverman, J., Herut, B., 2017. Interannual thermohaline (1979–2014) and nutrient (2002–2014) dynamics in the Levantine surface and intermediate water masses, SE Mediterranean Sea. Global and Planetary Change 151 (2017) 60–67. http://dx.doi.org/10.1016/j.gloplacha.2016.04.001

Pinardi, N., Bonazzi, A., Dobricic, S., Milliff, R.F., Wikle, C.K., Berliner, L.M., 2011. Ocean ensemble forecasting. Part II: Mediterranean forecast system response. Q. J. R. Meteorol. Soc. 137, 879–893.

Pinardi, N., Zavatarelli, M., Arneri, E., Crise, A., Ravaioli, M., 2006. The physical, sedimentary and ecological structure and variability of shelf areas in the Mediterranean Sea. In: Robinson, A.R., Brink, K. (Eds.), The Sea, vol. 14. Harvard University Press, Cambridge, USA, pp. 1245–1330.

Zodiatis, G., Drakopoulos, P., Brenner, S., Groom, S., 2005. Variability of Cyprus warm core eddy during the CYCLOPS project. Deep-Sea Res. 52, 2897–2910.

Zodiatis, G., Hayes, D., Gertman, I., Samuel-Rhoads, Y., 2010. The Cyprus warm eddy and the Atlantic water during the CYBO cruises (1995–2009). Rapp. Commun. Mer Mediterr. 39, 202.

Zodiatis, G., Theodorou, A., Demetropulos, A., 1998. Hydrography and circulation south of Cyprus in late summer 1995 and in spring 1996. Oceanol. Acta 21, 447–458.

6. Appendix

The gliders were programed to collect data throughout the dive/climb cycle every 10 seconds for pressure, temperature and conductivity and every 60 seconds for dissolved oxygen and optical parameters (backscatter 470 nm, backscatter 700 nm, chlorophyll—a fluorescence 470/690 nm). Dives were programmed for 1000m maximum depth, with altimeter configured so the glider could avoid the seafloor if less than 1000m. Optical parameters were sampled in the upper 600 m for most dives (unlike phase II which was to 300 m), and dissolved oxygen only in the upper 600 m (with exceptions for both at the beginning and the end of the missions for deep water reference). Due to the glider sampling design, upcast CTD observations miss the top 20 to 30 m depth. Figure A1 shows the histogram of the minimum depth value at which the CTD started to sample for (a) C2 and (b) C5 missions.

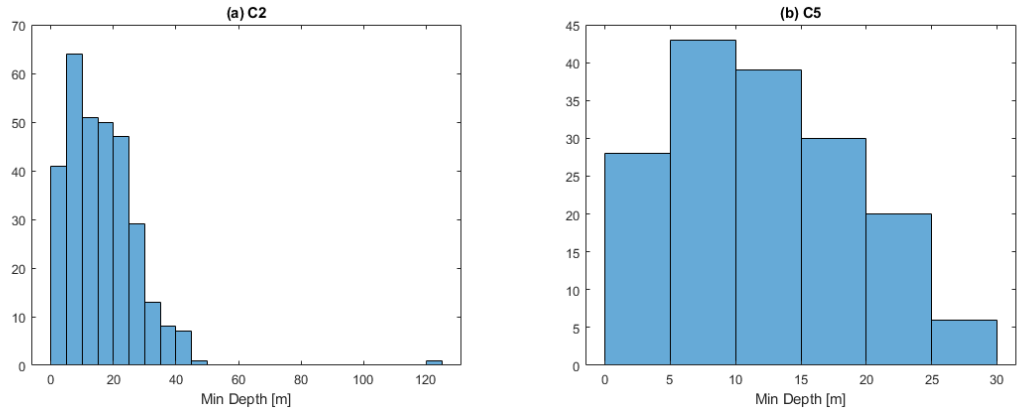

Figure A1. Histogram of the minimum depth value at which the CTD started to sample for (a) C2 and (b) C5 missions.